P8.8 THE STRUCTURE AND TIME EVOLUTION OF POLARIMETRIC SIGNATURES IN SEVERE CONVECTIVE STORMS: HIGH-RESOLUTION NUMERICAL SIMULATIONS AND DATA FROM A MOBILE, X-BAND DOPPLER RADAR

Jeffrey C. Snyder*, Howard B. Bluestein, Youngsun Jung
University of Oklahoma, Norman

Stephen Frasier and Vijay Venkatesh
University of Massachusetts, Amherst

1. INTRODUCTION

As the amount of polarimetric weather radar data collected in supercells continues to increase, numerous polarimetric signatures have been observed and described [e.g. Kumjian and Ryzhkov (2008) and Romine et al. (2008), amongst others]. Much of this past work, however, has been performed using S-band and C-band data, with the availability of X-band polarimetric, volumetric radar data of severe convective storms limited to only a handful of datasets up until the past few years. Though several signatures have been highlighted in the past, the physical processes behind such signatures are not necessarily well understood.

With the availability of a polarimetric radar simulator (Jung et al. 2010), output from high-resolution numerical models can now be examined in terms of commonly-used polarimetric weather radar products. It is with the simulator and convection-resolving model output that polarimetric signatures can be examined in an attempt to enhance the understanding of how these signatures arise within convective storms. *The results presented herein are very preliminary and represent the early stages of this study.*

Though the use of bulk microphysics far from perfectly models the microphysical processes that occur in deep moist convection, the use of multi-moment schemes has been shown [e.g. Dawson et al. (2010); Jung et al. (2010)] to better capture microphysical processes that occur within thunderstorms (e.g. sedimentation). The purpose of this study is not to examine the details of each simulation in a highly-quantitative manner, since even the three-moment scheme used in this study is imperfect. Rather, *this investigation is being performed in an attempt to extract meaningful signal from idealized simulations to provide insight into the physical processes behind some of the observed polarimetric signatures.*

* *Corresponding author address*: Jeffrey Snyder, School of Meteorology, University of Oklahoma
120 David L. Boren Blvd., Ste. 5355, Norman, OK 73072. Email: wxguy1@ou.edu

2. METHODS AND DATA

2.1 Instrument and Data Overview

The observational data used in this study were collected by the UMass X-Pol radar, a mobile, truck-mounted, dual-polarization (linearly polarized in the horizontal and vertical), X-band Doppler weather radar, built and maintained by the Microwave Remote Sensing Laboratory (MIRSL) at the University of Massachusetts – Amherst. Since 2002, graduate students and faculty at the University of Oklahoma, in collaboration with MIRSL, have used the UMass X-Pol throughout the central United States to collect data of severe convection (Fig. 1). Refer to Table 1 for selected characteristics of the radar; see Junyent-Lopez (2003) and Pazmany et al. (2003) for more detailed information.

Products available from the UMass X-Pol radar system include reflectivity at horizontal polarization (Z_H), differential reflectivity (Z_{DR}), radial velocity (V_R), total differential phase (Φ_{DP}), and the magnitude of the co-polar cross-correlation coefficient at zero lag (ρ_{HV}).

Scattering calculations indicate that attenuation and differential attenuation at X band may be nearly an order of magnitude greater than that at S band and several times that at X band. For some of the datasets collected, attenuation has been estimated using the ZPHI method (Testud et al. 2000), as described in Snyder et al. (2010). For consistency, since these estimates have not been performed for all datasets shown in this paper, the Z_H and Z_{DR} data presented herein do not account for the effects of attenuation. However, the observational facet of this project is most focused on mid- and upper-storm polarimetric signatures since the lower-tropospheric signatures (namely, the tornado debris signature and the Z_{DR} arc) evident in data collected by the UMass XPol have been examined by Bluestein et al. (2007a,b), Snyder (2008), and Snyder et al. (2010). As such, much of the data represent resolutions volumes above the environmental freezing level, where attenuation is generally much less significant.

The Φ_{DP} data were filtered [similar to Hubbert and Bringi (1995)] in an attempt to remove the backscatter differential phase component and to retrieve the propagation differential phase (ϕ_{DP}). Using ϕ_{DP}, K_{DP} was calculated by linear regression over a 1.5 km range.

Figure 1. The UMass XPol radar collecting data of a tornadic supercell in southeastern Wyoming in 2009. © J. Snyder

2.2 Simulations Overview

Numerous simulations were completed using the Advanced Regional Prediction Model (ARPS 5.3), a fully compressible, non-hydrostatic model designed and maintained by the Center for Analysis and Prediction of Storms (CAPS) at the University of Oklahoma. The three-moment microphysics scheme outlined in Milbrandt and Yau (2005a-b) has been added to ARPS and was used in this study; the use of multimoment bulk microphysics has been shown to yield more realistic convective storm simulations (e.g. Dawson et al. 2010). More details on the configuration of the model are available in Table 2. A polarimetric radar simulator (Jung et al. 2010) was used to examine the simulated convective storms in the context of common polarimetric radar products as would be seen by an X-band radar.

Physical Characteristics	
Operating Frequency	9.41 GHz
Antenna Diameter	1.8 m
Antenna Beamwidth	1.25° (3 dB)
Transmission Characteristics	
Peak Power (H+V)	25 kW (pre-2009) 12.5 kW (2009-10)
Pulse Length	1 µs
Range Resolution	150 m
PRF	1.6 kHz / 2.0 kHz
Receiving Characteristics	
Sampling Resolution	60 m (2007-2010)
Dynamic Range	~73 dB
Receiver Gain	~45 dB

Table 1. Selected characteristics of the UMass XPol.

Several simulations were completed, though limited results are presented at this time. Each simulation was run using a unique combination of one of two artificial thermodynamic soundings [based on the simple analytical model of Weisman and Klemp (1982)]

Model Configuration	
Model	ARPS v5.3
Horizontal Grid Spacing	500 m
Vertical Grid Spacing	Stretched; 100 m near surface, ~700 m near model top
Domain Size	203 x 203 x 53 (100 km x 100 km x 19 km)
Time Steps	Large: 2.0 s Small: 0.5 s
Computional Mixing	4th order in horizontal and vertical
Microphysics	Three-moment, five species (Milbrandt and Yau 2005a,b)
Turbulence Parameter.	Anisotropic 1.5 order TKE
Boundary Conditions	Lateral: radiation Bottom: Rigid Top: Rigid with Rayleigh damping
Initial Perturbation	Magnitude: 4 K Shape: 10 km x 10 km x 1.5 km centered 1.5 km AGL

Table 2. Model details and configuration.

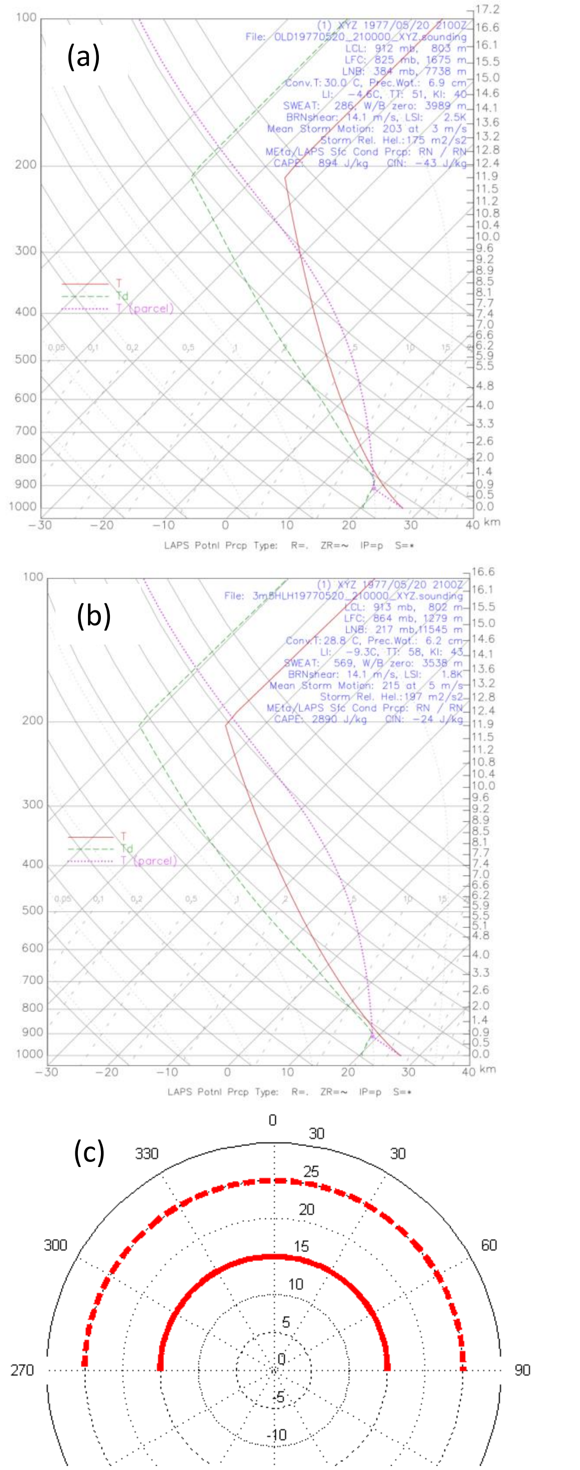

Figure 2. The low-CAPE (~900 j/kg SBCAPE) and high-CAPE (~2900 j/kg SBCAPE) thermodynamic profiles [(a) and (b), respectively] and (c) the hodographs (with constant veering of the wind with height from the surface to 10 km AGL) used as initial conditions in the four simulations. Rings in (c) have units of m s^{-1}.

and either of two hodographs. One of the goals of this work is to examine how different levels of CAPE affect the polarimetric representation of the modeled supercells; however, there are a nearly infinite number of ways to modify the thermodynamic characteristics of the troposphere to change CAPE. Certainly, different thermodynamic soundings will be examined for future simulations. In addition, the influence of the shape of the hodographs and the distribution of vertical shear through the troposphere will also be examined more thoroughly in future simulations.

3. POLARIMETRIC SIGNATURES

Several previous studies have noted various polarimetric signatures [e.g. Kumjian et al. (2008); Romine et al. (2008)], including Z_{DR} and K_{DP} towers, mid-level ρ_{hv} and Z_{DR} rings (or half-rings), Z_{DR} arcs, and probable hail signatures. However, most of the previous work has been performed using data collected at S and C bands, with relatively limited observations of polarimetric signatures at X band (and at the very high resolutions provided by many mobile radars such as the UMass XPol). As a result of resonance effects that are much more prominent at X band than at S band, as well as large resolution differences that exist between most of the polarimetric radars used in previous studies and the UMass XPol, it is expected that some of the polarimetric signatures presented previously in the literature may differ from what has been collected by this X-band radar.

3.1 Simulation results

Currently-understood polarimetric signatures have been primarily identified using observations, and the physical processes behind the signatures have been a mix of well-reasoned speculation and some simple modeling. However, it is difficult to understand completely the causative mechanisms responsible for the appearance of the various signatures based upon observations alone; a more detailed suite of atmospheric characteristics (e.g. vertical velocity, rainwater and hail mixing ratios, etc.) are not available using radar data in isolation.

Calculated Z_{DR} and ρ_{hv} data valid at t=3600 s in the high CAPE, low shear simulation (Fig. 3) exhibit two commonly-observed polarimetric signatures – the Z_{DR} tower and the ρ_{hv} ring. A vertical cross-section through the updraft of the modeled supercell (Fig. 3a) indicates a strong association between relatively high Z_{DR} above the ambient freezing level (~4 km AGL) and the updraft. In this case, the model is reproducing the often-seen Z_{DR} tower.

The calculated ρ_{hv} on a horizontal slice at 4875 m AGL through the supercell at the same time reveals what looks to be a ρ_{hv} ring (Fig. 4b). Surrounding the main part of the updraft (which is indicated by the 10-20+ m s^{-1} vertical velocities), there is a ring of reduced ρ_{hv}, with the value of ρ_{hv} quite variable around the periphery of the updraft. On the “inflow notch” side (i.e. the east and southeast side of the updraft in this case), calculated ρ_{hv} < 0.7, whereas it is closer to 0.88-0.92 along the remaining periphery of the updraft. Due to time constraints, we have not yet examined the mass concentrations or size distribution parameters for the hydrometeor species that are located within this ρ_{hv} ring, though this will be studied more thoroughly in future work.

Preliminary observations:

- The height of the Z_{DR} columns expectedly is higher in the high CAPE runs
- In general, the size (i.e. width) of the Z_{DR} columns is larger in the longer hodograph runs
- The mid-level ρ_{hv} rings are much better defined and are seen earlier in the storms’ lifetimes in the high CAPE simulations
- Very few instances of Z_{DR} rings are seen

Items that require attention:

- It appears that K_{DP} in areas of rain is sometimes much higher than expected. Whether this is the result of microphysics or a discrepancy in the K_{DP} calculation from model output will be investigated.
- In its current form, the three-moment scheme used with ARPS does not allow for a change in median drop diameter as a result of evaporation. The practical consequence of this on model simulations is not known.

3.2 Survey of observations

Since 2008, the UMass XPol has focused on collecting volumetric data (that is, data from near the surface to 8+ km AGL), allowing for the examination of structures within the polarimetric fields near and above the freezing level of many of the storms on which data were collected. For the most part, many of

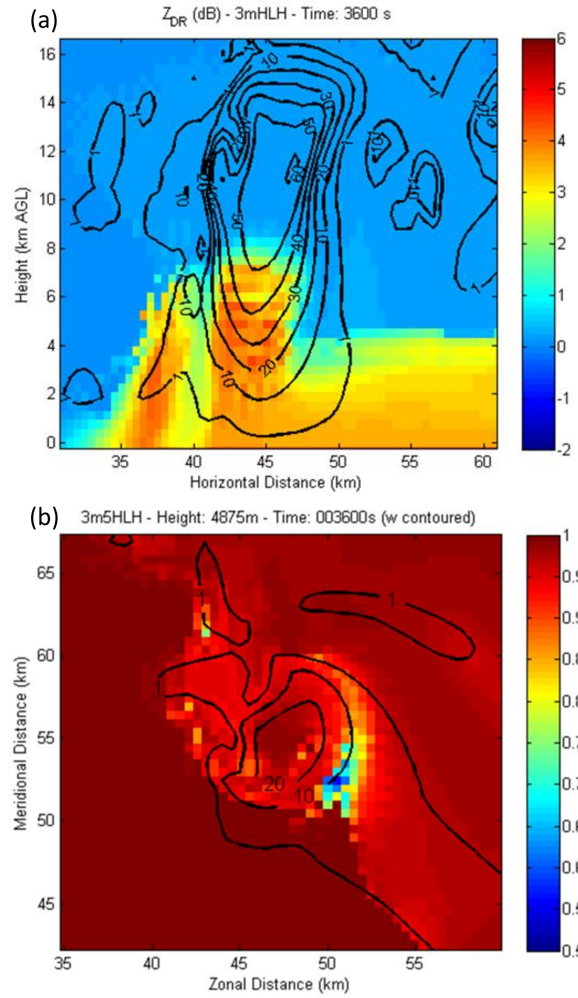

Figure 3. (a) Z_{DR} (color) and vertical velocity (contoured; m s^{-1}) on an X-Z cross-section through the supercell updraft in the high CAPE, low shear simulation capturing the Z_{DR} tower. From the same simulation, (b) a well-defined ρ_{hv} ring (color) is evident surrounding the updraft (vertical velocity – contoured; m s^{-1}) at a height of 4875 m above ground level (AGL)

the previously-seen polarimetric signatures are evident in various datasets collected by the UMass XPol (Fig. 4). For example, mid-level Z_{DR} rings or half-rings are quite obvious in data from 31 May 2007 (Fig. 4a), 18 May 2010 (Fig. 4c), and 22 May 2008 (Fig. 4e). In the first two, the Z_{DR} (half) rings are either completely closed or most prevalent on the “inflow” side of the weak or bounded weak echo region (BWER); in the third, there is very little echo overhang, WER, or BWER present.

Similar in location to the Z_{DR} (half) rings, mid-level ρ_{hv} rings are also evident in some of

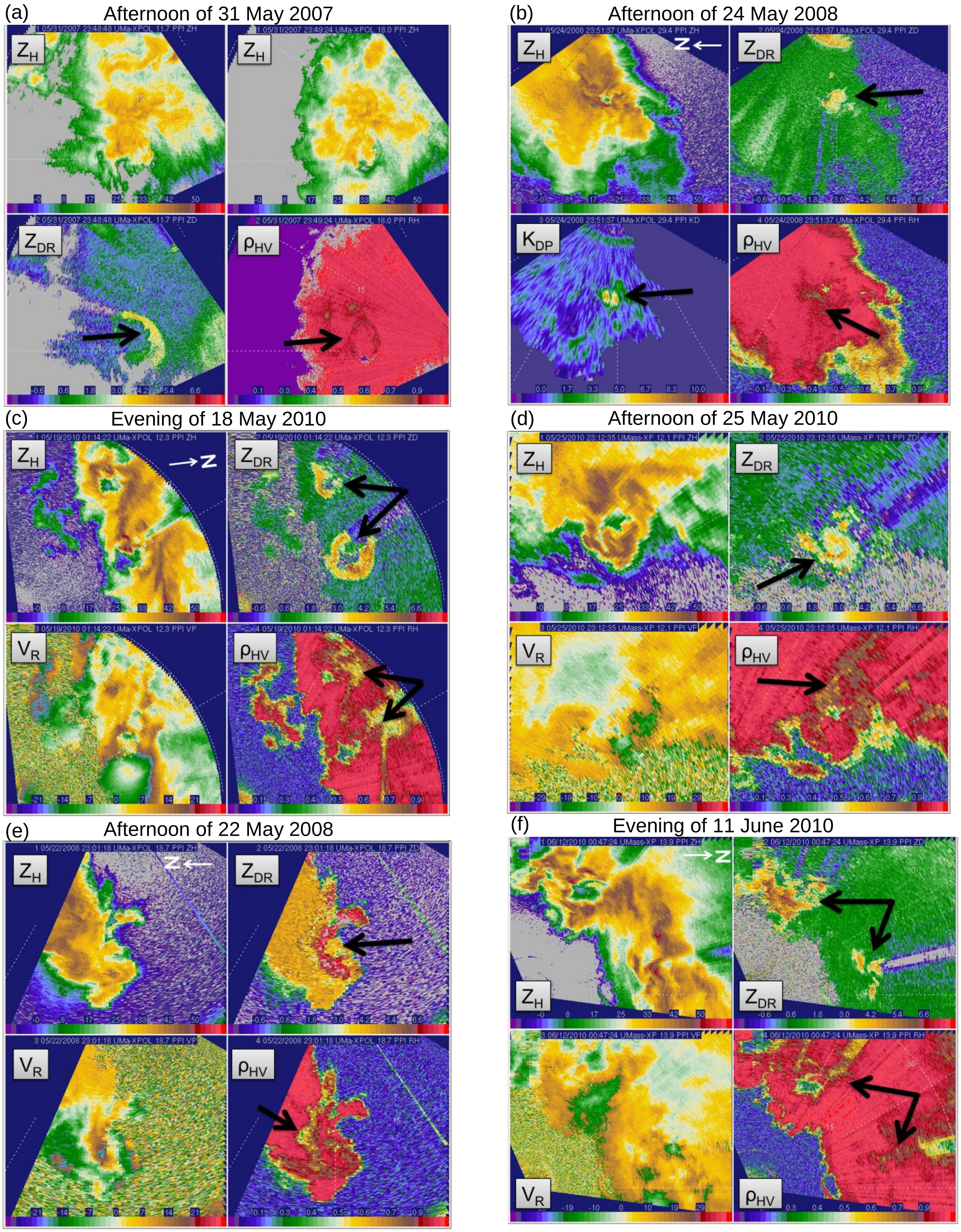

Figure 4. Observed polarimetric signatures, including Z_{DR} rings (a, c, e), ρ_{hv} rings (a, d, e), likely Z_{DR} towers (b, d, f), and ρ_{hv} minima to the NW-NE of BWERs (a, b, c, d, f). North is "up" unless otherwise indicated. In (a), the two images in the left and right columns are valid at slightly different times and elevation angles.

the data. Illustrative of this, a complete ρ_{hv} ring can be seen in Fig. 4a and a ρ_{hv} half-ring in Fig. 4e. In some of the other dates and scans represented in Fig. 4, there are some indications of reduced ρ_{hv} near the BWER.

Consistent with previous observations (Kumjian and Ryzhkov 2008), evidence of Z_{DR} towers is apparent even in the PPI images as areas of Z_{DR} > 1 dB at heights well above the ambient freezing level, the result of partially-liquid hydrometeors in the relatively warm updrafts between the ambient freezing level and the updraft-perturbed freezing level. For example, in panels b, d, and f of Fig. 4, Z_{DR} > 3 dB is apparent very nearly collocated with the BWERs and, if the BWER is highly correlated with the location of the updraft, the updrafts. Similarly, the presence of a K_{DP} tower is evident in Fig. 4b as K_{DP} > 5 deg. km^{-1} is nearly collocated with the small BWER and the area of positive Z_{DR} tower.

3.2.1 Reduced mid-level ρ_{hv} left of BWER

The evolution of a BWER observed on 17 May 2010 in southeastern New Mexico also reveals some interesting changes in the ρ_{hv} data (Fig. 5). At 2117 UTC, the BWER is oval-shaped (Fig. 5a), with the major axis oriented approximately WSW-ENE. Through the next eight minutes (Fig. 5c,e,f), the BWER deforms greatly, progressively become more "U"-shaped with time such that, by 2129 UTC (Fig. 5e), the BWER is nearly open on the south side.

Radial velocity data (not shown) indicate strong inbounds on the northwest side of the BWER, which may have been the cause for distortion of the BWER with time. The ρ_{hv} data also indicate the presence of the BWER; the very low ρ_{hv} in the BWER is likely the result of noise bias associated with very low signal-to-noise ratio (SNR). However, the reduced ρ_{hv} at 2117 UTC (Fig. 5b) is nearly "T"-shaped; the southern area of low ρ_{hv} is associated with the BWER, but a large part of the northern area is characterized by Z_H > 40 dBZ. As the BWER (as seen in the Z_H data) deforms, so too does the area of reduced ρ_{hv}. Through this time, however, the northern area of lowered ρ_{hv} is collocated with Z_H of at least 35 dBZ. This area of ρ_{hv} < 0.7 and Z_H > 30 dBZ to the left (in a storm relative sense, or to the north in this particular case) of the BWER may indicate the presence of large quantities of mixed-phase hydrometeors (wet hail, graupel, etc.).

Other examples of very low ρ_{hv} to the left of the BWER are found in UMass XPol data. For example, an area of ρ_{hv} < 0.8 and Z_H > 30 dBZ is evident to the left of a crescent-shaped BWER on 31 May 2007 (Fig. 6a,b). Similarly-low ρ_{hv} in areas of Z_H > 30 dBZ on the left side of (or to the left of) the updraft is evident in data from 5 June 2009 (Fig. 6c-f), as well as in nearly all cases in Fig. 5.

3.2.2 Low reflectivity ribbon

A narrow band of locally-reduced Z_H extending from near where the hook echo "attaches" to the main body of the echo associated with the rear of the forward-flank downdraft has been observed in at least several supercells (Fig. 7) on which the UMass XPol collected data; this feature is most evident in the lower troposphere. In data from 5 June 2009

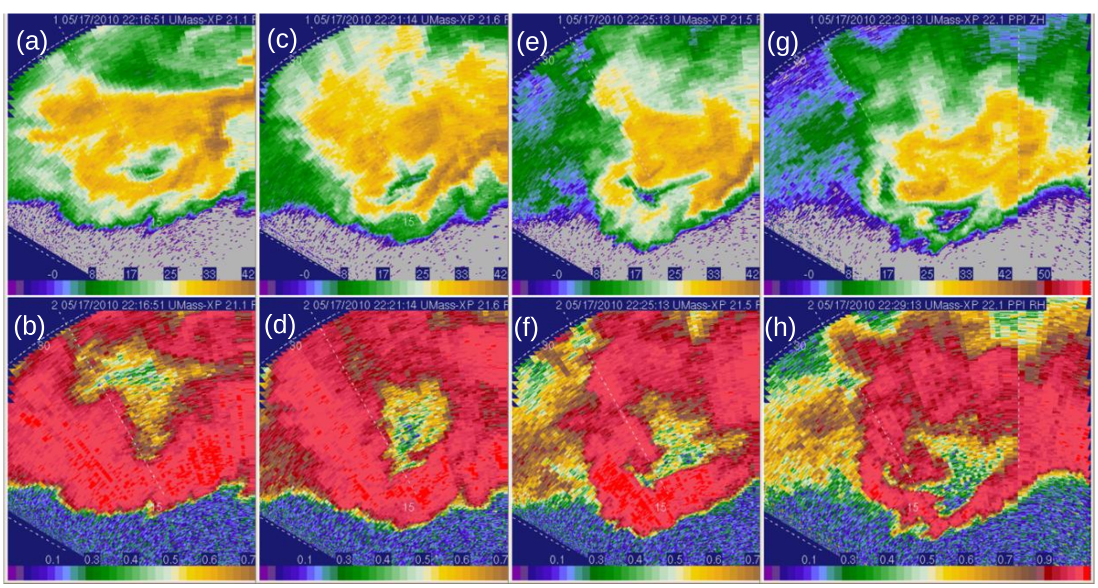

Figure 5. The evolution of the BWER on 5/17/2010 as seen in Z_H (top row) and ρ_{hv} (bottom row) at approximately 4 minute intervals (2117 UTC, 2121 UTC, 2125 UTC, and 2129 UTC, left to right) on the 21-22º elevation angle scan.

Figure 6. (a) Z_H and (b) ρ_{hv} data from 5/31/2007 valid at 13.4º; (c) Z_H, (d) radial velocity, (e) Z_{DR}, and (f) ρ_{hv} from 6/5/2009 at 12.9º. Note the presence of very low ρ_{hv} in (b) to the NW of the BWER, even where Z_H is >30 dBZ.

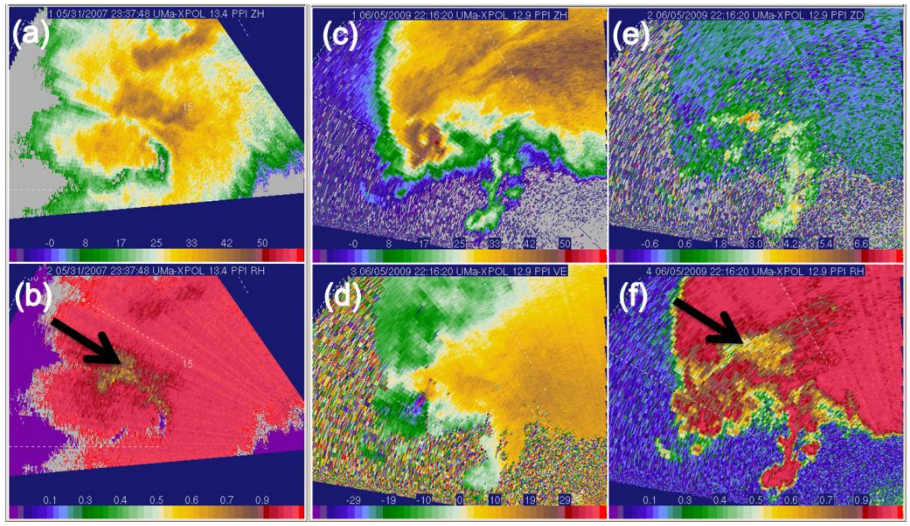

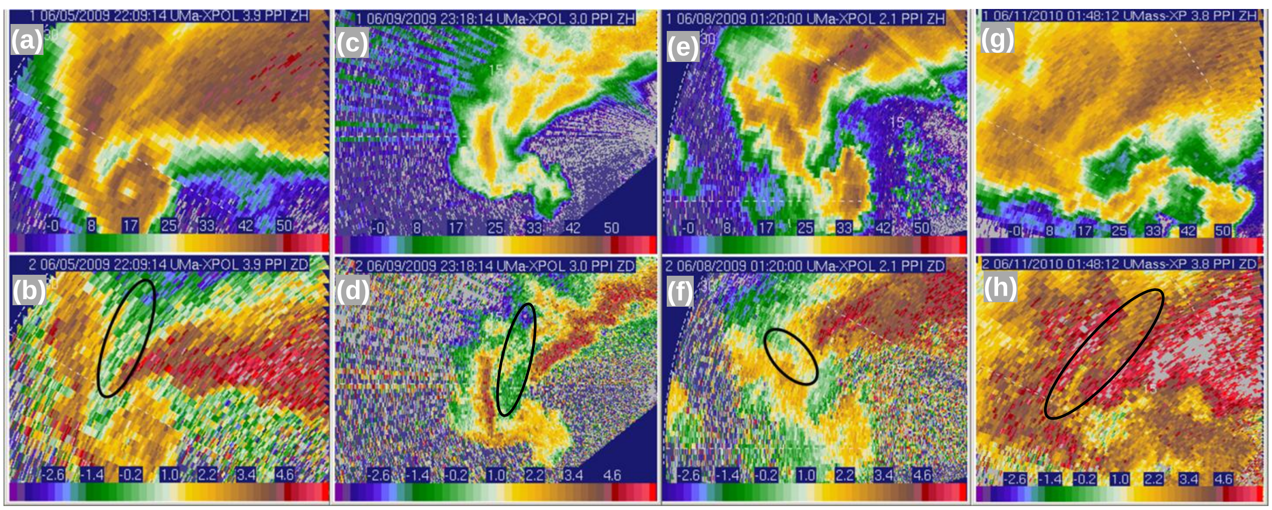

Figure 7. Z_H (top) and Z_{DR} (bottom) from, left to right, 6/5/09, 6/9/09, 6/7/09, and 6/10/10. Note a narrow band of lowered Z_H and Z_{DR} near the location where the hook echoes "attach" to the main body of the echo. These plots are not of attenuation-corrected data.

(Fig. 7a-b) and 10 June 2010 (Fig. 7g-h), a ribbon of relatively low Z_H extends northeastward from near the area where the hook echo appears to "attach" the main body of the storm on the upshear side of the FFD. On 9 June 2009 (Fig. 7c-d) and 7 June 2009 (Fig. 7e-f), a ribbon of low ZH exists in similar storm-relative locations, but the ribbons are aligned in a more N-S or NW-SE orientation.

Associated with the ribbon of reduced Z_H is a ribbon of reduced Z_{DR}. In three of the supercells, the measured Z_{DR} minima are largely in the 0-1 dB range (Fig. 7b,d,f); in the other supercell (Fig. 7h), the locally-reduced Z_{DR} is ~2 dB. The radial velocity and ρ_{hv} data (not shown) do not contain organized anomalies in these "low reflectivity ribbons", though a much more thorough examination of these data is warranted and will occur in the near future.

In terms of the characteristics of various hydrometeors that are typically associated with parameter values in the ranges seen in these "low reflectivity ribbons", it seems possible that these features represent areas of rain drop-size distributions (DSDs) whose mean drop size is significantly smaller than surrounding areas. In this vein, it may be prudent to examine disdrometer data near these features, if available (Dawson and Romine 2010). In addition, these ribbons may represent a sort of hail signature. As to why they have not been pointed out in the past, it seems plausible that, considering their relatively narrow nature, the observing radar system must be able to collect high-resolution data. Perhaps, too, as a result of resonance effects, these features are particularly evident at X band.

Many questions about this feature remain. What, if anything, does this feature tell us about the dynamics or organization of these particular supercells? What hydrometeors constitute the scatterers in these ribbons? Is there are relationship between these ribbons and tornadogenesis? These questions, as well as others, will be examined in future work.

4. CONCLUSIONS

The images presented herein represent the very beginning stages of a more thorough examination into the time evolution of polarimetric signatures using X-band radar data and high-resolution numerical model output. The results from four simulations indicate the various polarimetric signatures seen in observed data (e.g. Z_{DR} and K_{DP} towers and ρ_{hv} rings) are captured by the simulated radar data from numerical model output. Future work will continue to examine the role of shear and CAPE on the polarimetric representation (and the time evolution of such representation) of supercells using various hodographs and soundings, and the role of other model characteristics (e.g. microphysical schemes and grid spacing) on the retrieved polarimetric representations will be investigated.

5. ACKNOWLEDGMENTS

This work was supported under NSF grants ATM-0637148 and ATM-0934307 awarded to the University of Oklahoma, and ATM-0242166 and ATM-0641201 awarded to the University of Massachusetts – Amherst. The computing for this project was performed at the OU Supercomputing Center for Education & Research (OSCER) at the University of Oklahoma (OU). The authors wish to thank Dan Dawson for consultation and assistance in the design of the simulations.

6. REFERENCES

Bluestein, H. B., M. M. French, R. L. Tanamachi, S. Frasier, K. Hardwick, F. Junyent, and A. L. Pazmany, 2007a: Close-range observations of tornadoes in supercells made with a dual-polarization, X-band, mobile Doppler radar. *Mon. Wea. Rev.,* **135,** 1522-1543.

——, C. C. Weiss, M. M. French, E. M. Holthaus, R. L. Tanamachi, S. Frasier, and A. L. Pazmany, 2007b: The structure of tornadoes near Attica, Kansas, on 12 May 2004: High-resolution, mobile, Doppler radar observations. *Mon. Wea. Rev.,* **135,** 475-506.

Dawson, D. T., and G. Romine, 2010: A preliminary survey of DSD measurements collected during VORTEX2. Preprints, *25th Conference of Severe Local Storms,* Denver, CO, Amer. Meteor. Soc., 8A.4. [Available online at http://ams.confex.com/ams/pdfpapers/176115.pdf]

Dawson, D. T., M. Xue, J. A. Milbrandt, and M. K. Yau, 2010: Comparison of evaporation and cold pool development between single-moment and multimoment bulk microphysics schemes in idealized simulations of tornadic thunderstorms. *Mon. Wea. Rev.,* **138,** 1152-1171.

Hubbert, J., and V. N. Bringi, 1995: An iterative filtering technique for the analysis of copolar differential phase and dual-frequency radar measurements. *J. Atmos. Oceanic Technol.,* **12,** 643-648.

Jung, Y., M. Xue, and G. Zhang, 2010: Simulations of polarimetric radar signatures of a supercell storm using a two-moment bulk microphysics scheme. *J. Appl. Met. Climatol.,* **49,** 146-163.

Junyent-Lopez, F. J., 2003: The design, development, and initial field deployment of an X-band polarimetric Doppler weather radar. M. S. thesis, Electrical and Computer Engineering, University of Massachusetts Amherst, 120 pp.

Kumjian, M. R., and A. V. Ryzhkov, 2008: Polarimetric signatures in supercell thunderstorms. *J. Appl. Met. Climatol.,* **47,** 1940-1961.

Milbrandt, J. A., and M. K. Yau, 2005a: A multi-moment bulk microphysics parameterization. Part I: Analysis of the role of the spectral shape parameter. *J. Atmos. Sci.,* **62,** 3051–3064.

——, and ——, 2005b: A multi-moment bulk microphysics parameterization. Part II: A proposed three-moment closure and scheme description. *J. Atmos. Sci.,* **62,** 3065–3081.

Pazmany, A. L., F. J. Lopez, H. B. Bluestein, and M. Kramar, 2003: Quantitative rain measurements with a mobile, X-band, polarimetric Doppler radar. Preprints, *31st*

Conference on Radar Meteorology, Seattle, WA, American Meteorological Society, 858-859.

Romine, G. S., D. W. Burgess, and R. B. Wilhelmson, 2008: A dual-polarization-radar-based assessment of the 8 May 2003 Oklahoma City area tornadic supercell. *Mon. Wea. Rev.,* **136,** 2849-2870.

Snyder, J. C., 2008: Attenuation correction techniques and hydrometeor classification of high-resolution, X-band, dual-polarized mobile radar data of severe convective storms. M. S. thesis, Meteorology, University of Massachusetts Amherst, 148 pp. [Available from School of Meteorology, University of Oklahoma, 120 David L. Boren Blvd., Norman, OK 73072].

Snyder, J. C., H. B. Bluestein, G. Zhang, and S.J. Frasier, 2010: Attenuation correction and hydrometeor classification of high-resolution, X-band, dual-polarized mobile radar measurements in severe convective storms. *J. Oceanic Technol.* (in press).

Testud, J., E. Le Bouar, E. Obligis, and M. Ali-Mehenni, 2000: The rain profiling algorithm applied to polarimetric weather radar. *J. Atmos. Oceanic Technol.,* **17,** 332-356.

Weisman, M. L., and J. B. Klemp, 1982: The dependence of numerically simulation convective storms on vertical wind shear and buoyancy. *Mon. Wea. Rev.,* **110,** 504-520.